Threshold Dynamics of a Semiconductor Single Atom Maser

Y.-Y. Liu,[1] J. Stehlik,[1] C. Eichler,[1] X. Mi,[1] T. R. Hartke,[1] M. J. Gullans,[2] J. M. Taylor,[2] and J. R. Petta[1]
[1]Department of Physics, Princeton University, Princeton, New Jersey 08544, USA
[2]Joint Quantum Institute and Joint Center for Quantum Information and Computer Science, NIST and University of Maryland, College Park, Maryland 20742, USA
(Received 6 April 2017; published 31 August 2017)

We demonstrate a single atom maser consisting of a semiconductor double quantum dot (DQD) that is embedded in a high-quality-factor microwave cavity. A finite bias drives the DQD out of equilibrium, resulting in sequential single electron tunneling and masing. We develop a dynamic tuning protocol that allows us to controllably increase the time-averaged repumping rate of the DQD at a fixed level detuning, and quantitatively study the transition through the masing threshold. We further examine the crossover from incoherent to coherent emission by measuring the photon statistics across the masing transition. The observed threshold behavior is in agreement with an existing single atom maser theory when small corrections from lead emission are taken into account.

DOI: 10.1103/PhysRevLett.119.097702

Examining photon emission from single quantum emitters provides a window into the interaction between light and matter. The first single atom maser was realized by passing single Rydberg atoms—which provided a transient gain medium—through a superconducting cavity [1]. The cavity quantum electrodynamics (QED) approach provides a template for a variety of single emitter lasing experiments involving optical cavities that are coupled to either natural or artificial atoms [2–5]. Of particular interest is the observation of nonclassical optical phenomena, such as Fock state generation and thresholdless lasing [2–6]. Circuit QED has enabled dramatic improvements in the coupling between solid-state devices and microwaves, with the demonstration of single photon sources, tomography of itinerant photon states, and the stabilization of cat states of light [7–10]. An on-chip single atom amplifier and maser have also been demonstrated using superconducting junctions [11,12].

Semiconductor double quantum dots (DQDs) have been placed in microwave cavities with charge-cavity coupling rates $g_c/2\pi = 10$–100 MHz [13–17], and the strong-coupling regime has recently been achieved [18–20]. DQDs allow a great level of experimental control, as their energy-level structure is electrically tunable [21,22]. Furthermore, nonequilibrium physics can be explored by applying a source-drain bias across the DQD or by periodically driving the energy level detuning ϵ [16,23,24]. These characteristics have enabled a wide range of quantum optics experiments with DQDs, such as photon emission between hybridized single-electron states [25–27]. Masing can be observed in these systems when the gain exceeds the loss, as recently demonstrated by placing two voltage-biased InAs DQDs in a microwave cavity [23].

In this Letter, we examine the threshold dynamics of a semiconductor single atom maser (SeSAM) consisting of a single DQD that is embedded in a microwave cavity and driven by single electron tunneling events. In contrast with previous experiments that required multiple emitters to exceed the masing threshold [23], we demonstrate masing with a single DQD emitter through improvements in the cavity quality factor Q_c and g_c. We introduce a dynamic tuning protocol that changes the effective repumping rate of the DQD, allowing us to directly observe the transition from below threshold, where the system is dominated by incoherent emission, to above threshold, where the emission is coherent. The threshold behavior is in qualitative agreement with a single atom maser theory from atomic physics [6]. We obtain quantitative agreement with the data by including photoemission events that originate from tunneling between the DQD and the source-drain electrodes [26,28–31].

The SeSAM consists of a DQD that is embedded in a half-wavelength $\lambda/2$ superconducting cavity [Fig. 1(a)]. The cavity has a resonance frequency $f_c = 7.5$ GHz and total decay rate $\kappa_{\mathrm{tot}}/2\pi = 1.5$ MHz. The inset of Fig. 1(a) shows a scanning electron microscope (SEM) image of a single InAs nanowire that is placed on top of 5 metallic gates that are electrically biased to form a double-well confinement potential along the length of the nanowire [32]. Charges trapped in the double well have a dipole moment that directly interacts with the cavity field, resulting in a large $g_c/2\pi \approx 70$ MHz [14,24,25].

In comparison with previous work, we can achieve masing with a single DQD emitter [14,25]. The experiment has been improved by reducing microwave leakage through dc gate biasing lines and increasing g_c by fabricating devices with a smaller gap between the source and drain electrodes [24]. Quantitatively, the competition between loss κ_{tot} and gain Γ_{spon} can be defined using the normalized inversion ratio $r = \Gamma_{\mathrm{spon}}/\kappa_{\mathrm{tot}}$ [25]. Considering the first-order photon emission plus the phonon-assisted photon emission process, we find $r \propto g_c^2 Q_c$ [26,33]. When $r > 1$, maser action is triggered. In a previous experiment we

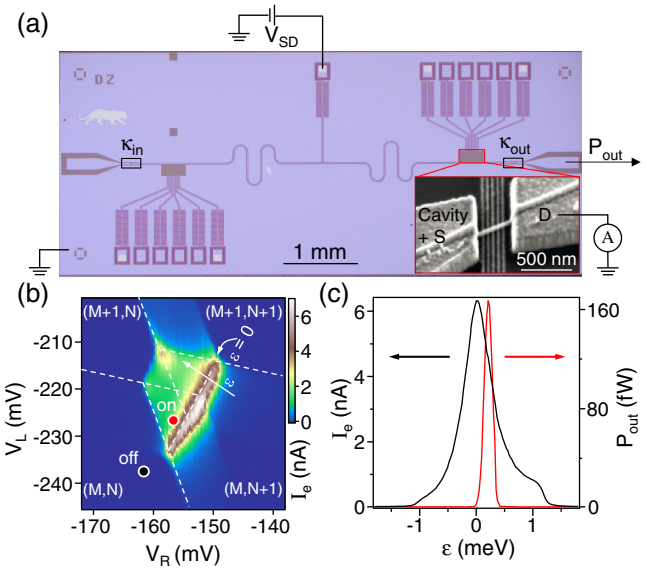

FIG. 1. (a) Optical micrograph of the DQD SeSAM. The source-drain bias V_{SD} is applied through an LC filtered bias tee. The cavity is connected to input and output ports with coupling rates κ_{in} and κ_{out}. Inset: SEM image of an InAs nanowire DQD. (b) I_e as a function of V_L and V_R with $V_{SD} = 2$ mV. (c) I_e (black) and P_{out} (red) plotted as a function of ϵ.

achieved a maximum $r \sim 0.75$ with a single DQD [25]. With the present device, Q_c and g_c have been improved by a factor of 2; thus, we expect $r > 1$ and the device to exceed the masing threshold.

The SeSAM is powered by a source-drain bias $V_{SD} = 2$ mV that is applied to the DQD via the LC filtered bias tee connected to the cavity voltage node [34]. Figure 1(b) shows the resulting current I_e as a function of the gate voltages V_L and V_R. Charge states are labeled (N_L, N_R), where $N_{L(R)}$ indicates the electron number in the left (right) dot. Sequential tunneling events are only allowed within the finite bias triangles [as delineated by the dashed lines in Fig. 1(b)]. Cotunneling current is observed outside of the finite bias triangles due to the large tunnel coupling to the leads. As shown in previous work, interdot tunneling leads to photon emission into the cavity mode [25–27,29]. The resulting cavity field is probed by measuring the power emitted from the cavity output port P_{out} using heterodyne detection (see Ref. [24] for measurement details).

Evidence for photon emission due to electron tunneling is shown in Fig. 1(c), where P_{out} and I_e are plotted as a function of DQD energy level detuning ϵ. The source-drain bias results in a peak current of 6 nA at $\epsilon = 0$, where the left and right dot energy levels are resonant. In contrast, the output power peaks at $\epsilon = 0.3$ meV, where the current $I_{on} = 4$ nA and $P_{out} = 160$ fW. The source-drain bias repumps the DQD to the excited state at a rate $|I_e/e|$ and generates the population inversion required for stimulated emission, similar to masing experiments involving Cooper pair boxes [35]. For the conditions that result in the maximum output

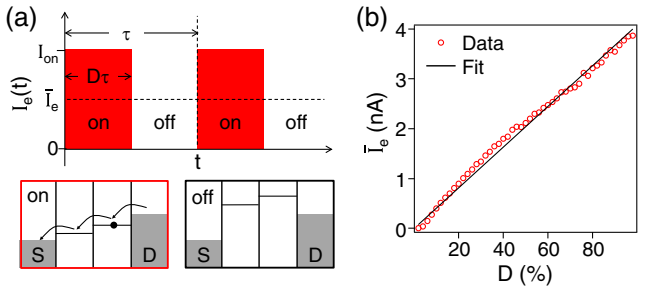

FIG. 2. (a) Upper panel: Pulse sequence used to tune the time-averaged current flowing through the device. A square wave with a period $\tau = 50$ ns and duty cycle D is applied to toggle the current on and off. The resulting time-averaged current is $\bar{I}_e = DI_{on}$. Lower panel: DQD level configuration with the current on (left panel) and off (right panel). (b) The measured $\bar{I}_e$ (red circles) as a function of D. The solid line is the prediction $\bar{I}_e = DI_{on}$.

power, the level detuning is approximately 9 times the cavity photon energy (30 μeV for a 7.5-GHz cavity). Previous theoretical work has examined the detuning dependence of the important elements leading to masing (e.g., charge-cavity coupling, population inversion, rapid repumping) and indicates that electron-phonon coupling is important in InAs nanowires, leading to an emission process where a phonon and photon are simultaneously emitted [26].

The strong emission that is observed is suggestive of above-threshold masing that is triggered by current flow through a single DQD. The emission spectrum (not shown) has a linewidth of 11 kHz, corresponding to a coherence time of 30 μs [23]. To investigate the threshold behavior we now measure the statistics of the emitted microwave field as a function of repump rate. In conventional solid-state lasers, such as a diode laser, threshold behavior is studied by measuring the emitted power as a function of dc biasing conditions. Such an approach is not directly applicable to DQD devices since the resonant current (and, therefore, the repump rate) is independent of V_{SD} once the DQD energy levels are within the transport window [21]. Moreover, tuning the tunnel rates also changes the DQD energy level structure and g_c. We therefore develop a dynamic tuning process that changes the time-averaged current through the DQD.

As schematically illustrated in Fig. 2(a), a square wave with a period $\tau = 50$ ns and duty cycle D is applied to both the left and right gates to toggle the electron current on and off while keeping ϵ fixed. The locations of the "on" and "off" states in the stability diagram are indicated by the red and black dots in Fig. 1(b) and the corresponding energy level configurations are shown in the lower insets of Fig. 2(a). In the off state, the square-wave amplitude is selected such that the DQD energy levels are at least 1 meV from the Fermi level of the source and drain. As such, photon-assisted tunneling is highly suppressed in the off state. The time-averaged current through the DQD, $\bar{I}_e$, is plotted as a function of D in Fig. 2(b). As expected, the measured current scales linearly with D.

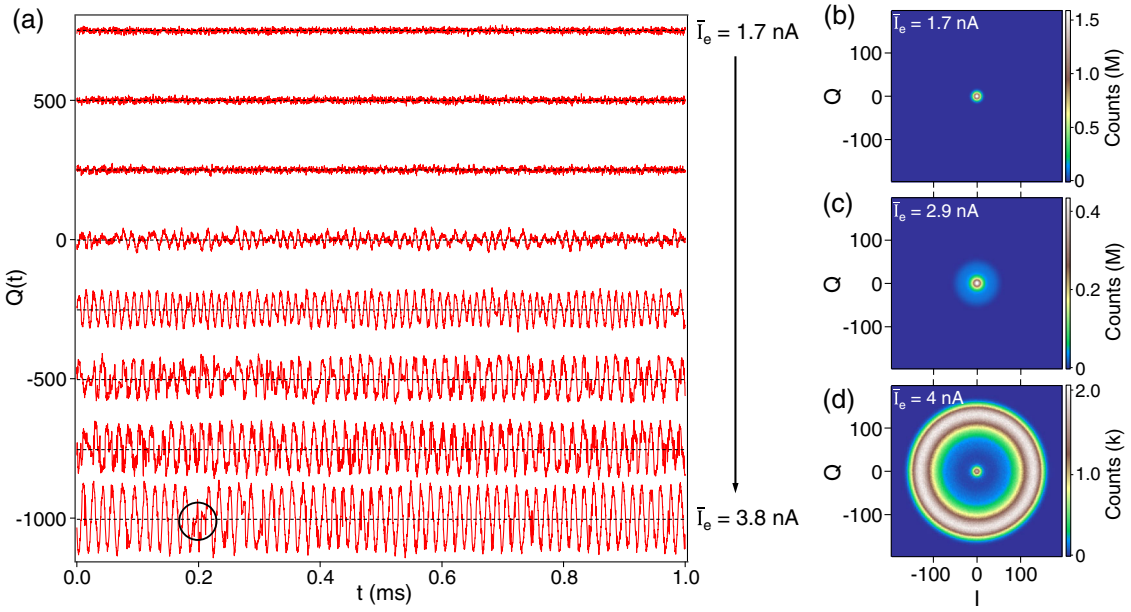

FIG. 3. (a) Time series $Q(t)$ with $\bar{I}_e$ ranging from 1.7 nA to 3.8 nA with a step size of 0.3 nA. The data are offset along the x axis by 250 in Q for clarity. The emission amplitude increases with increasing $\bar{I}_e$. (b)–(d) IQ histograms acquired with $\bar{I}_e = 1.7$, 2.9, and 4 nA. (b) The emission is centered around $(I, Q) = (0, 0)$ at small currents. (c) The distribution gradually broadens as $\bar{I}_e$ is increased. (d) With $\bar{I}_e = 4$ nA, the histogram has a ring shape indicative of above-threshold maser emission.

The dynamic tuning process is effective at setting the repump rate because $\kappa_{\text{tot}}/2\pi = f_c/Q_c = 1.5$ MHz is much less than the tunneling rate through the DQD, $I_{\text{on}}/|e| \approx 25$ GHz. Because of the fact that photon emission is driven by single electron tunneling events, the effective repump rate is proportional to the average current when $|e|/|I_{\text{on}}| \ll \tau < 1/\kappa_{\text{tot}}$ [33].

The time series of the demodulated quadrature-phase component of the cavity field $Q(t)$ qualitatively illustrates the crossover from below-threshold to above-threshold behavior as $\bar{I}_e$ is increased [Fig. 3(a)]. When $\bar{I}_e < 2.5$ nA the output is thermal noise, which is mainly attributed to background noise in the amplification chain. When $\bar{I}_e > 2.5$ nA, periodic voltage oscillations become visible, with an amplitude that increases with $\bar{I}_e$. The oscillating field is indicative of coherent emission. We note that the maser occasionally blinks off even for large $\bar{I}_e$ (see, for example, $t = 0.2$ ms at $\bar{I}_e = 3.8$ nA). We attribute the blinking to large charge fluctuations that shift the DQD level detuning [23]. Similar behavior has been observed in other solid-state lasers [36]. These data show that the dynamical detuning method effectively changes the DQD repump rate.

The maser emission statistics can be quantitatively studied by measuring histograms of the output field as a function of increasing $\bar{I}_e$. For each value of $\bar{I}_e$, we sample the in-phase and quadrature-phase components of the cavity field (I and Q) at a rate of 12.3 MHz and then plot 1.7×10^7 samples in a two-dimensional histogram [23,24]. Histograms with $\bar{I}_e = 1.7$, 2.9, and 4 nA are plotted in Figs. 3(b)–3(d). With a small current of $\bar{I}_e = 1.7$ nA, the histogram is centered within a narrow range of the origin in the IQ plane, as the detected field is dominated by the detection background noise. With increasing current, $\bar{I}_e = 2.9$ nA, the histogram broadens out into a larger range as shown in Fig. 3(c). For $\bar{I}_e = 4$ nA ($D = 100\%$), the IQ histogram has a ring shape that is indicative of above-threshold maser emission [Fig. 3(d)] and a small thermal component around $(I, Q) = (0, 0)$. As noted in previous work, the events around $(I, Q) = (0, 0)$ in Fig. 3(d) are attributed to blinking events that are visible in the time-series data (circled in black) of Fig. 3(a) [23]. These events account for only 0.8% of the total emission, a factor of 3 less than in our previous work with two DQD emitters in a cavity [23].

Measurements of P_{out} also provide insight into the threshold behavior and can be compared with existing single atom maser theories [6]. Figure 4 plots P_{out} as a function of $\bar{I}_e$ for two different devices. Focusing on Fig. 4(a), for small $\bar{I}_e = 1.5$ nA we measure $P_{\text{out}} \approx 10^{-5}$ pW. P_{out} gradually increases with increasing $\bar{I}_e$ until $\bar{I}_e \approx 2.5$ nA. There is a dramatic factor of ≈ 50 increase in P_{out} in the range $2.5 < \bar{I}_e < 2.8$ nA. For $\bar{I}_e > 2.8$ nA we find that P_{out} increases slowly again with $\bar{I}_e$. These data indicate that the maser crosses threshold when $\bar{I}_e \approx 2.5 \sim 2.8$ nA and is well above threshold for $\bar{I}_e > 2.8$ nA.

We can understand the threshold behavior with an expanded form of the semiclassical theory of a single-atom laser [6]. In particular, we model the DQD SeSAM using semiclassical laser equations that account for photon

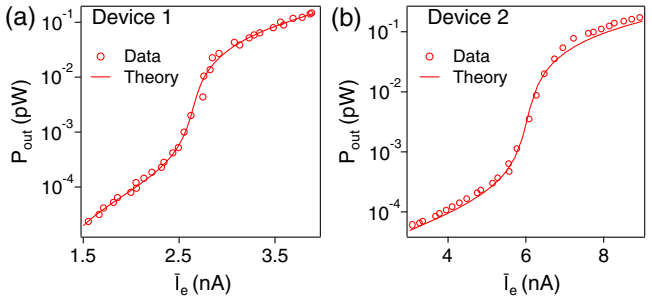

FIG. 4. P_{out} (red circles) as a function of $\bar{I}_e$ and fits to theory (solid lines) for two different devices. (a) Device 1 crosses threshold around $\bar{I}_e \approx 2.6$ nA. (b) Device 2 crosses threshold around $\bar{I}_e \approx 6.1$ nA. Both devices exhibit qualitatively similar threshold behavior.

emission events during interdot tunneling, as well as during tunneling onto and off of the leads,

$$\dot{u} = -[\gamma + \Gamma_p(n_c) + R]u + \Gamma_p(n_c) - Rn_c u, \quad (1)$$

$$\dot{n}_c = -\kappa_{\mathrm{tot}} n_c + Rn_c u + Ru + [\Gamma_p(n_c) - \Gamma_p^0](1-u), \quad (2)$$

$$\Gamma_p(n_c) = [1 + \alpha(n_c + 1)]\Gamma_p^0, \quad (3)$$

where u is the population of the state with one electron in the right dot and n_c is the intracavity photon number (see Fig. 2), $\Gamma_p(n_c)$ is the tunneling rate between the source-drain electrodes and the DQD states, Γ_p^0 is the bare tunneling rate, α is the fraction of lead tunneling events that result in photon emission, γ is the decay rate of the upper state of the DQD into modes (e.g., phonons) other than the cavity, R is the photon emission rate from the upper state of the DQD, and κ_{tot} is the total cavity decay rate. The dependence of the lead tunneling on cavity photon number arises from photon-assisted tunneling events between the leads and the DQD. When $\alpha = 0$, Eqs. (1)–(3) reduce to the conventional semiclassical theory of the single atom laser [6]. Spontaneous emission is accounted for by the terms where R and α appear independently of n_c.

We model the tuning cycle by coarse graining Eqs. (1)–(2) over one period with a duty cycle D, which effectively replaces u in Eq. (2) by Du. Similarly, we model the average current through the DQD as $\bar{I}_e = eD(\gamma + R + Rn_c)u$. The crucial parameter that relates $\bar{I}_e$ to P_{out} is the fraction of electron tunneling events through the DQD that result in photon emission, which we define as β. β will be influenced by the phonon sideband physics described by Gullans *et al.* [26]. We can estimate β by noting that the threshold current in our model is given by $I_{\mathrm{th}} = |e|\kappa_{\mathrm{tot}}/\beta$ with $\beta = R/\gamma + 2\alpha$. The full expression for P_{out} is derived in the Supplemental Material [33],

$$P_{\mathrm{out}} = \frac{G_{\mathrm{out}}^T}{G_{\mathrm{out}}^E}\frac{hf_c\kappa_{\mathrm{out}}}{2\xi R/\gamma}\left[\frac{\bar{I}_e}{I_{\mathrm{th}}} - 1 + \sqrt{\left(\frac{\bar{I}_e}{I_{\mathrm{th}}} - 1\right)^2 + \frac{4\xi\bar{I}_e}{I_{\mathrm{th}}}}\right]. \quad (4)$$

TABLE I. Fit parameters for the threshold behavior in Fig. 4.

		Device 1	Device 2
Measured parameters	f_c	7.5 GHz	7.6 GHz
	$\kappa_{\mathrm{tot}}/2\pi$	1.5 MHz	1.8 MHz
Calibrated	G_{out}^E	74.5 dB	72.8 dB
Free parameters	G_{out}^T	76.3 dB	76.2 dB
	I_{th}	2.63 nA	6.14 nA
	α	1.2×10^{-4}	0.3×10^{-4}
Calculated	$\beta = \kappa_{\mathrm{tot}}/\lvert e\rvert I_{\mathrm{th}}$	5.7×10^{-4}	2.9×10^{-4}
	$R/\gamma = \beta - 2\alpha$	3.3×10^{-4}	2.3×10^{-4}

κ_{out} is the coupling rate to the output port of the cavity and is designed to be $\kappa_{\mathrm{out}}/2\pi = 0.8$ MHz for both devices. Here we have also defined a correction parameter associated with the lead emission $\xi = 1 - 2\alpha\bar{I}_e/|e|\kappa_{\mathrm{tot}}$. The prefactor $G_{\mathrm{out}}^T/G_{\mathrm{out}}^E$ accounts for the systematic error in the total gain of the detection chain, G_{out}^E.

The theoretical prediction is in good agreement with data from two devices, as shown in Fig. 4. Fit parameters are listed in Table I. From calibrations of the amplifier gain, and room-temperature measurements of the losses in the coaxial lines, we estimate the total gain of the amplification chain to be $G_{\mathrm{out}}^E = 74.5$ dB for device 1, and $G_{\mathrm{out}}^E = 72.8$ dB for device 2 in another cooldown. Given experimental uncertainties in κ_{out}, losses in the device packaging, and the temperature-dependent losses in the coaxial lines, these values are in overall agreement with the best-fit value $G_{\mathrm{out}}^T = 76.3$ dB for device 1 and $G_{\mathrm{out}}^T = 76.2$ dB for device 2 [24,37]. The quantitative agreement of this model with the data suggests that lead emission events play an important role in the charge-cavity dynamics of our device [26,28–31]. The reader is referred to the Supplemental Material for a comparison to the standard single atom laser theory, which does not account for lead emission [33].

In conclusion, we have measured the threshold dynamics of a semiconductor single atom maser, which allows for investigations of maser physics in the simplest case of a single emitter in a cavity. Photon emission in the SeSAM is generated by single electron tunneling events. By implementing a dynamic tuning protocol, we quantitatively analyze the behavior of the SeSAM as it crosses threshold. The data are in agreement with a modified single atom maser theory that includes a correction due to lead emission.

Research was supported by the Gordon and Betty Moore Foundation's EPiQS Initiative through Grant No. GBMF4535, with partial support from the National Science Foundation through Grant No. DMR-1409556. Devices were fabricated in the Princeton University Quantum Device Nanofabrication Laboratory.

[1] D. Meschede, H. Walther, and G. Müller, One-Atom Maser, Phys. Rev. Lett. **54**, 551 (1985).

[2] J. McKeever, A. Boca, A. D. Boozer, J. R. Buck, and H. J. Kimble, Experimental realization of a one-atom laser in the regime of strong coupling, Nature (London) **425**, 268 (2003).

[3] S. Reitzenstein, T. Heindel, C. Kistner, A. Rahimi-Iman, C. Schneider, S. Höfling, and A. Forchel, Low threshold electrically pumped quantum dot-micropillar lasers, Appl. Phys. Lett. **93**, 061104 (2008).

[4] F. Dubin, C. Russo, H. G. Barros, A. Stute, C. Becher, P. O. Schmidt, and R. Blatt, Quantum to classical transition in a single-ion laser, Nat. Phys. **6**, 350 (2010).

[5] S. Haroche, Nobel lecture: Controlling photons in a box and exploring the quantum to classical boundary, Rev. Mod. Phys. **85**, 1083 (2013).

[6] P. R. Rice and H. J. Carmichael, Photon statistics of a cavity-QED laser: A comment on the laser-phase-transition analogy, Phys. Rev. A **50**, 4318 (1994).

[7] D. Bozyigit *et al.*, Antibunching of microwave-frequency photons observed in correlation measurements using linear detectors, Nat. Phys. **7**, 154 (2011).

[8] M. Hofheinz *et al.*, Synthesizing arbitrary quantum states in a superconducting resonator, Nature (London) **459**, 546 (2009).

[9] M. Hofheinz, E. M. Weig, M. Ansmann, R. C. Bialczak, E. Lucero, M. Neeley, A. D. O'Connell, H. Wang, J. M. Martinis, and A. N. Cleland, Generation of Fock states in a superconducting quantum circuit, Nature (London) **454**, 310 (2008).

[10] B. Vlastakis, G. Kirchmair, Z. Leghtas, S. E. Nigg, L. Frunzio, S. M. Girvin, M. Mirrahimi, M. H. Devoret, and R. J. Schoelkopf, Deterministically encoding quantum information using 100-photon Schrödinger cat states, Science **342**, 607 (2013).

[11] O. V. Astafiev, A. A. Abdumalikov, A. M. Zagoskin, Y. A. Pashkin, Y. Nakamura, and J. S. Tsai, Ultimate On-Chip Quantum Amplifier, Phys. Rev. Lett. **104**, 183603 (2010).

[12] O. Astafiev, K. Inomata, A. O. Niskanen, T. Yamamoto, Y. A. Pashkin, Y. Nakamura, and J. S. Tsai, Single artificial-atom lasing, Nature (London) **449**, 588 (2007).

[13] T. Frey, P. J. Leek, M. Beck, A. Blais, T. Ihn, K. Ensslin, and A. Wallraff, Dipole Coupling of a Double Quantum Dot to a Microwave Resonator, Phys. Rev. Lett. **108**, 046807 (2012).

[14] K. D. Petersson, L. W. McFaul, M. D. Schroer, M. Jung, J. M. Taylor, A. A. Houck, and J. R. Petta, Circuit quantum electrodynamics with a spin qubit, Nature (London) **490**, 380 (2012).

[15] H. Toida, T. Nakajima, and S. Komiyama, Vacuum Rabi Splitting in a Semiconductor Circuit QED System, Phys. Rev. Lett. **110**, 066802 (2013).

[16] J. J. Viennot, M. R. Delbecq, M. C. Dartiailh, A. Cottet, and T. Kontos, Out-of-equilibrium charge dynamics in a hybrid circuit quantum electrodynamics architecture, Phys. Rev. B **89**, 165404 (2014).

[17] G.-W. Deng *et al.*, Charge Number Dependence of the Dephasing Rates of a Graphene Double Quantum Dot in a Circuit QED Architecture, Phys. Rev. Lett. **115**, 126804 (2015).

[18] X. Mi, J. V. Cady, D. M. Zajac, P. W. Deelman, and J. R. Petta, Strong coupling of a single electron in silicon to a microwave photon, Science **355**, 156 (2017).

[19] A. Stockklauser, P. Scarlino, J. V. Koski, S. Gasparinetti, C. K. Andersen, C. Reichl, W. Wegscheider, T. Ihn, K. Ensslin, and A. Wallraff, Strong Coupling Cavity QED with Gate-Defined Double Quantum Dots Enabled by a High Impedance Resonator, Phys. Rev. X **7**, 011030 (2017).

[20] L. E. Bruhat, T. Cubaynes, J. J. Viennot, M. C. Dartiailh, M. M. Desjardins, A. Cottet, and T. Kontos, Strong coupling between an electron in a quantum dot circuit and a photon in a cavity, arXiv:1612.05214.

[21] W. G. van der Wiel, S. De Franceschi, J. M. Elzerman, T. Fujisawa, S. Tarucha, and L. P. Kouwenhoven, Electron transport through double quantum dots, Rev. Mod. Phys. **75**, 1 (2002).

[22] T. Fujisawa, T. H. Oosterkamp, W. G. van der Wiel, B. W. Broer, R. Aguado, S. Tarucha, and L. P. Kouwenhoven, Spontaneous emission spectrum in double quantum dot devices, Science **282**, 932 (1998).

[23] Y.-Y. Liu, J. Stehlik, C. Eichler, M. J. Gullans, J. M. Taylor, and J. R. Petta, Semiconductor double quantum dot micromaser, Science **347**, 285 (2015).

[24] J. Stehlik, Y.-Y. Liu, C. Eichler, T. R. Hartke, X. Mi, M. J. Gullans, J. M. Taylor, and J. R. Petta, Double Quantum Dot Floquet Gain Medium, Phys. Rev. X **6**, 041027 (2016).

[25] Y.-Y. Liu, K. D. Petersson, J. Stehlik, J. M. Taylor, and J. R. Petta, Photon Emission from a Cavity-Coupled Double Quantum Dot, Phys. Rev. Lett. **113**, 036801 (2014).

[26] M. J. Gullans, Y.-Y. Liu, J. Stehlik, J. R. Petta, and J. M. Taylor, Phonon-Assisted Gain in a Semiconductor Double Quantum Dot Maser, Phys. Rev. Lett. **114**, 196802 (2015).

[27] A. Stockklauser, V. F. Maisi, J. Basset, K. Cujia, C. Reichl, W. Wegscheider, T. Ihn, A. Wallraff, and K. Ensslin, Microwave Emission from Hybridized States in a Semiconductor Charge Qubit, Phys. Rev. Lett. **115**, 046802 (2015).

[28] L. Childress, A. S. Sørensen, and M. D. Lukin, Mesoscopic cavity quantum electrodynamics with quantum dots, Phys. Rev. A **69**, 042302 (2004).

[29] P.-Q. Jin, M. Marthaler, J. H. Cole, A. Shnirman, and G. Schön, Lasing and transport in a quantum-dot resonator circuit, Phys. Rev. B **84**, 035322 (2011).

[30] M. Kulkarni, O. Cotlet, and H. E. Türeci, Cavity-coupled double-quantum dot at finite bias: Analogy with lasers and beyond, Phys. Rev. B **90**, 125402 (2014).

[31] C. Müller and T. M. Stace, Deriving Lindblad master equations with Keldysh diagrams: Correlated gain and loss in higher order perturbation theory, Phys. Rev. A **95**, 013847 (2017).

[32] S. Nadj-Perge, S. M. Frolov, E. P. A. M. Bakkers, and L. P. Kouwenhoven, Spin-orbit qubit in a semiconductor nanowire, Nature (London) **468**, 1084 (2010).

[33] See Supplemental Material at http://link.aps.org/supplemental/10.1103/PhysRevLett.119.097702 for details of the theoretical model.

[34] X. Mi, J. V. Cady, D. M. Zajac, J. Stehlik, L. F. Edge, and J. R. Petta, Circuit quantum electrodynamics architecture for gate-defined quantum dots in silicon, Appl. Phys. Lett. **110**, 043502 (2017).

[35] S. Ashhab, J. R. Johansson, A. M. Zagoskin, and F. Nori, Single-artificial-atom lasing using a voltage-biased superconducting charge qubit, New J. Phys. **11**, 023030 (2009).

[36] S. E. Siegman, *Lasers* (University Science Books, Mill Valley, 1986).

[37] Y.-Y. Liu, J. Stehlik, M. J. Gullans, J. M. Taylor, and J. R. Petta, Injection locking of a semiconductor double-quantum-dot micromaser, Phys. Rev. A **92**, 053802 (2015).